euspen's 26th International Conference & Exhibition, Krakow, PL, June 2026
www.euspen.eu

Voxel-Scale Misalignment Detection for Orthogonal Metasurface-produced Holograms via Error-Compensated Volumetric Imaging

Gavin Stafford[1], Timothy Yap[2], Michael Cullinan [1]

[1,2]*The University of Texas at Austin, Walker Department of Mechanical Engineering*

ghstaff@utexas.edu

Abstract

Metasurfaces are thin diffractive optical elements composed of subwavelength structures that can alter the amplitude, phase, and/or polarization of incoming light. These structures can be tuned to reconstruct a 3D light intensity pattern composed of voxels, input as a computer-generated hologram (CGH), within a photocurable resin. This metasurface-based additive manufacturing process, much like conventional projection lithography, is limited in its axial resolution by the square of the NA (numerical aperture) of the optical system. However, with the addition of a second, orthogonal metasurface, and careful tuning of light intensity and resin chemistry, photopolymerization can be localized to only those regions enclosed by the voxels of both metasurface projections simultaneously, improving the axial resolution. To make this orthogonal curing possible, the voxels of the two projected holograms must overlap, meaning that alignment at the scale of the voxel is necessary. To achieve this, we introduce an error-compensated volumetric imaging system for misalignment detection and correction. The system uses four-focal-length relays to transport both hologram images from their locations within the sample volume to a CMOS (Complementary metal-oxide-semiconductor) sensor mounted on a precision stage, which determines their relative displacement and orientation. A calibration artifact is used to compensate for systematic error in this process through imaging of its features along both arms. By comparing the CMOS-imaged relative feature locations to the actual relative feature locations of the target, a transformation matrix for each arm can be calculated that incorporates systematic error in the relays. These matrices will allow future closed-loop feedback control of the hologram alignment by mapping the volumetric imaging captured by the CMOS to misalignment values, which can then be plugged into the motorized stage of the moveable metasurface to bring the two holograms into alignment.

Additive Manufacturing, Metasurfaces, Alignment, Lithography

1. Introduction

Traditionally, holographic lithography is done as a variable process, in which holograms are rapidly encoded into an SLM (spatial light modulator) in order to change the projected light intensity pattern. This is done with tomographic 2D projections in the case of computed axial lithography [1], as well as with multi-foci projections [2] in order to produce volumetric prints. While adaptable, these processes are inherently limited in the optical resolution they can achieve due to the large minimum pixel size of SLMs. Metasurfaces, on the contrary, cannot be changed in their design once printed, but are limited in their pixel size only by the feature resolution capabilities of their fabricating device. This allows for much smaller pixels, and thus a much higher achievable optical resolution. Moreover, fabrication methods for metasurfaces are arbitrarily scalable, such as TPA (two-photon absorption) printing, meaning that the size of the metasurface can be increased to permit the desired volumetric throughput of the metasurface lithographic process while maintaining optical resolution, provided the stitching between fabrication regions of the metasurface does not affect the produced hologram.

Metasurfaces, while reaching higher resolution than SLMs, still suffer from low resolution along the optical axis, where the square of the NA limits the spatial confinement of light. To overcome this hurdle, a method of overlapping orthogonal holograms is introduced, for the purpose of only curing within a desired overlapping volume. This requires precise overlap of the target holograms. This paper presents a novel misalignment detection method based off of registering each hologram with a common reference target, and using this common frame to calculate the centroidal displacement of the two holograms. These misalignment values can be used in future work to correctly align and print with orthogonal metasurfaces.

These metasurfaces are made using an optical inverse design algorithm, as shown in Figure 1, which takes a 3D shape, slices it into planes, and optimizes a phase mask such that the intensity of the electromagnetic field it produces best matches those planes. This mask is then fabricated and used for vat photo-polymerization.

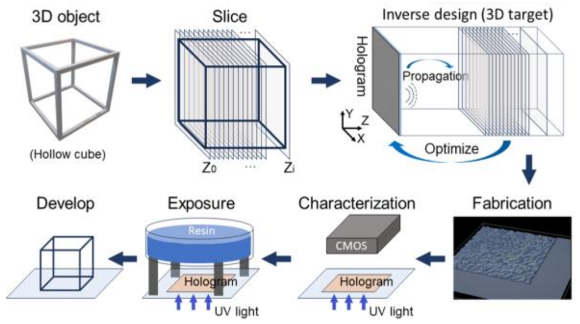

Figure 1. Holographic Metasurface Lithography Process

2. Methodology

2.1. Optical Setup

Alignment of the holograms starts with the illumination of the phase mask by a uniform, coherent light source. The optical system used is built to deliver this coherent source to the mask at normal incidence, and with full coverage. Figure 2 shows the CAD of the optical setup, which was replicated in the lab. The 405 nm coherent laser source is aligned, filtered and magnified, and finally passed through the phase masks.

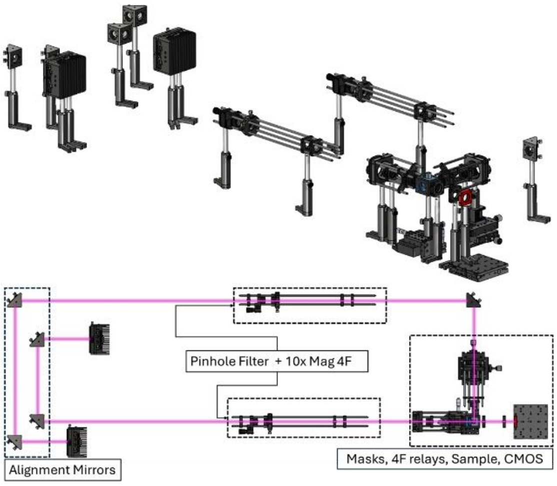

Figure 2. CAD of Illumination Optics

Figure 3 shows a close up view of the phase mask projection assembly, where 4f (4-focal-length) lens relays are used to relay the cube-shaped holograms produced by the masks to the sample/target stage.

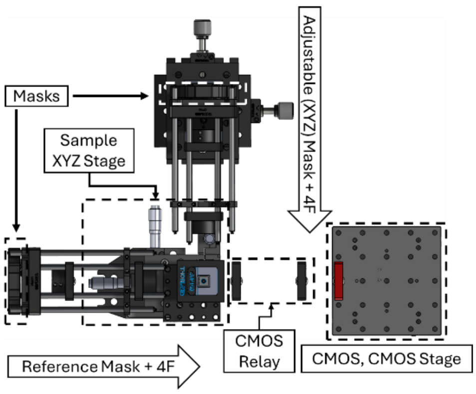

Figure 3. CAD of Sample/Target Stage Area

This is a zero magnification relay done solely to arbitrarily increase the projection distance of the phase masks from their designed 3 mm. These projected holograms are designed as point clouds, or "gaussian dot" approach, with these dots being 2-3 pixels in diameter, effectively acting as 10-15 µm voxels. The sample cuvette holder is shown on the XYZ stage, which is present when doing printing. Figure 4 shows a picture of this sample XYZ stage with a calibration target and diffuser in place, which are used for the focus scanning. The axes labelled in this figure are the "global" axes by which the final hologram misalignments will be defined. This figure also shows the 4f relays that relay the hologram images from the sample or target frame to the CMOS detector. These are composed of two 1 inch diameter, 30 mm focal length achromatic lenses.

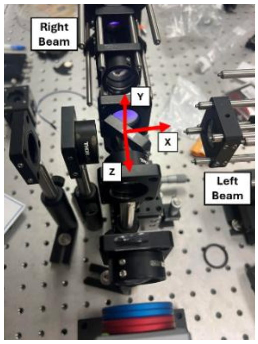

Figure 4. Sample XYZ Stage with Diffuser and Calibration Target

2.2. Checkerboard Scanning, Focus Scoring

Once there is confidence in the illumination optics, the alignment scheme is started. It consists of a mirrored process, where the left hologram is scanned and removed, then the calibration target is placed, and the left focus scanning is done for two sample stage locations. The CMOS is then moved opposite the right beam, and completes the focus scanning for that axis at two sample stage locations. Finally, the right hologram is inserted and scanned. This mirrored process of scanning hologram, target, target, hologram is implemented such that each hologram is tied to its respective focus scan, and the focus scans are tied to one another through the calibration target. Any other order would fail the registration of the holograms with their scans, or the scans with one another, as the target must be removed to scan the holograms. The movement of the sample stage to two different locations for each focus scan is necessary to satisfy the non-coplanarity requirement for a set of points that defined a 3D rigid body transformation.

This focus scanning process moves the image relayed to the CMOS across the angled calibration target and maps which X coordinates (5.5 µm pixels on the CMOS) contain the most in focus corners of the calibration grid, at that Z location. The resulting XYZ point coordinates are recorded, and matched with their pair of coordinates in the target frame, which is easily calculated due to the known width of the target squares (250 µm). These points are shown in Figure 5 for single frames within the each of the 4 scans of the checkerboard.

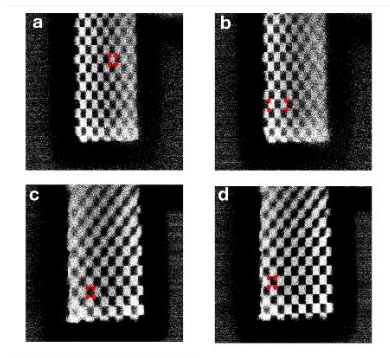

Figure 5. Corners of Interest in: (a) First Left Scan (b) Second Left Scan (c) First Right Scan (d) Second Right Scan

When initially scanning the angled calibration target along the Z axis, there was a large range (5 mm +) where the squares had little aperture diffraction, thus it was difficult to use the minimum of this aperture diffraction as a measurement of focus, as originally planned. The solution to this was placing a diffuser in front of the target, which scatters the illuminating light before it hits the target, drastically increasing the range of illumination angles. This decreased the range where the checkerboard was in focus enough for the shift in focus along the screen to become obvious as the Z location of the CMOS changed.

The metric used to determine this focus was the Binary Shannon Entropy of the 4 quadrants surrounding each corner of interest, as shown in Figure 6.

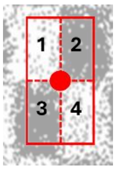

Figure 6. Quadrants for Shannon Entropy Calculation

Shannon entropy, defined in Eq. 1 for the binary images it evaluates, calculates the information density of a region. For a given region, this roughly equates to the number of variables necessary to fully define it. For example, a cup of coffee with cream sitting on top as a single layer would have low Shannon entropy, and as it is mixed, its Shannon entropy would grow larger and larger as more variables would be necessary to define the position of the cream as it mixes into the coffee. In the case of the checkerboard, for a perfectly black pixel or white pixel quadrant, the Shannon entropy would be at a minimum, and for a region of completely intermixed and random black and white pixels, the Shannon entropy would be at a maximum. This score is defined in Eq. 2, where the entropy of the surrounding quadrants is averaged to give an accurate representation of the focus at the corner.

$$H(Q_i) = -[p \log_2 p + (1-p) \log_2 (1-p)] \quad (1)$$

Where H is the Shannon entropy, Q is the quadrant, and p is the probability of a black (or white) pixel. This probability is what is scraped from the image.

$$Focus\ Score = 1 - \frac{\sum_{i=1}^{4} H(Q_i)}{4} \quad (2)$$

Each scan consisted of 80 2048×2048 pixel images spaced at intervals of 20um. Videos of these scans were made in order to watch and qualitatively determine which grid corners went from defocus, to focus, and again to defocus within the scan. These corners were then selected for the Shannon entropy algorithm to evaluate. A graph of this focus score along the Z scan is shown in Figure 6, where two points, Peak 3 and Peak 4, were selected due to their superior peak spacing, which closely resembled that expected, based on the tilt angle of the target (measured by comparing the width of the squares in the image to their actual 250 µm width).

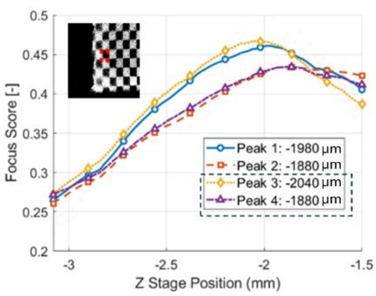

Figure 6. Focus Score Curves for 4 Points Along the Second Right Scan

Even though Peak 1 and Peak 2 have almost the same focus curves, their calculated peaks are not spaced adequately for fitting to the periodicity of the angled target. A 25 scan wide average was applied to these curves to eliminate random noise and deduce the overall focus trend. This is how all of the 4 CMOS – target point pairs were found for each of the 4 scans, yielding the 8 sets of points for each transformation.

The hardware error budget for the scanning procedure is shown in Table 1, where the most contributing factor is the large focus sampling interval of 20 µm, which was chosen for speed. This can, in the future, be decreased down to the repeatability of the CMOS stage, 1 µm. The resulting RMS error value due to the hardware was 23.07 µm.

Table 1. Hardware Error Budget for Focus Scanning

CMOS Pixel Resolution [µm]	5.5
CMOS Stage Bi-Directional Repeatability [µm]	± 1
Target Stage Bi-Directional Repeatability [µm]	±10
Target Grid Resolution [µm]	1
Focus Sampling Interval Resolution [µm]	20

2.3. Frame Transformations

The 4f relays for the CMOS were aligned carefully before use so that the CMOS to target transforms could be defined by rigid transformations instead of affine transformations. This was done with a mind to the large hardware RMS error present, as an affine transform, with its extra degrees of freedom, could overfit to that random error.

The method used to determine the best rigid transform matrix was a Procrustes analysis that optimized the rotation and translation matrices between frames to minimize the RMS error of the transform, which is shown in Eq. 3.

$$E_{rigid} = \sqrt{\frac{1}{n}\sum_{i=1}^{n} \|T_i - (RS_i - t)\|^2} \quad (3)$$

Where E_{rigid} is the RMS error of the rigid transform, T_i is the current point in the CMOS frame, S_i is the point pair in the target frame, R is the rotation matrix, and t is the translation vector.

Once these transformations are calculated, one for the left beam and one for the right beam, the left and right holograms themselves are scanned for transformation. This is done by identifying visually the start and end planes of each hologram, and generating points for their corners, such that a cube can be defined for each. These planes are shown in Figure 7.

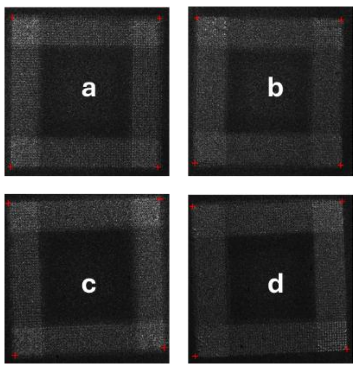

Figure 7. CMOS Images of Start/End Hologram Planes (a) Left Start (b) Left End (c) Right Start (d) Right End

3. Results

The results of the rigid transformation optimization produced transforms with RMS errors shown in Table 2.

Table 2. RMS Error of Left and Right Rigid Transforms

RMS Error, Left Transform [µm]	RMS Error, Right Transform [µm]
45.81	30.43

These values being higher than the hardware RMS indicate that there is also non-trivial error in the Shannon entropy focus finding algorithm. Once performed on the cube representations of the holograms, their misalignment in the global reference frame can be calculated as shown in Table 3 and visualized as shown in Figure 8, where the cubes represent the holograms, and the tails on these cubes represent the direction the light travels from.

Table 3. Misalignment Values in the Global Reference Frame (Note: Values reference the coordinate frame shown in figure 8)

Misalignment X [µm]	Misalignment Y [µm]	Misalignment Z [µm]
-2377.84	207.98	2361.52

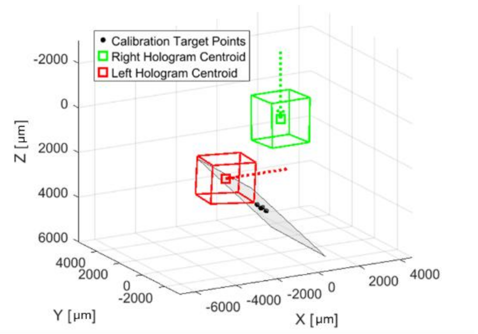

Figure 8. Misalignment of Cubes in 3D with Calibration Target as Reference

4. Discussion

The RMS error inherent to the calculated transforms is partially due to the hardware and scan interval, and partially due to the inability of the Shannon entropy-based focus algorithm to accurately track the focus shift. This was not a narrow band of focus, nor was it sharp. Instead, it was a few squares wide, and dropped off over the course of 1-2 squares. With the width of the tilted squares being 150-200 µm depending on the tilt angle, this meant an effective area of focus almost 1 mm wide, discernable by the human eye, as seen in Figure 5. The Shannon entropy image processing allows a much tighter evaluation of the focus along the checkerboard than this 1mm band, as it quantitatively discerns differences in the entropy of a point as the focus band moves over it, allowing the identification of a peak of focus. This is solely for finding valid points for the geometric transforms, which when applied to each hologram, give their relative displacements in a common reference frame. Therefore, this 1mm focus band has absolutely no bearing on the range of misalignment values that can be detected. It will only influence the RMS errors of the transforms it informs. For a tighter band of focus, a higher NA lens should be used to gather higher incoming angles of light, and a lower grit diffuser should be used to scatter at those higher angles. The addition of a diffuser is what made the focus shift sensitive enough for the Shannon entropy measure to track, so a diffuser with more scatterability could increase that shift sensitivity even more. Additionally, the high scanning interval of 20 µm can be decreased to drastically improve the hardware RMS error. These are the two most effective ways to eventually get single digit micron alignment with this method.

The misalignment values (Table 3) indicate exactly why this method was necessary. The Y misalignment is small because it is possible to visually align the two holograms within a couple hundred µm in this axis by using a fluorescent card. The large X and Z misalignments of 2 mm are the result of an inability to accurately probe the location of the hologram peak planes along its optical axis with a fluorescent card, as the human eye cannot discern the subtle changes in contrast that occur from plane to plane. A qualitative alignment scheme was previously implemented that used the calibration target as a beam combination as half of the squares are reflective. This showed both holograms on a CMOS at the same time, which allowed for them to be aligned along the global Y axis and the CMOS X axis. The trouble is that this CMOS X axis did not correspond to either of the global X or Z axes, because of the reflection transformation on the hologram. They simply couldn't be aligned effectively with the CMOS along their optical axes, because if they weren't sitting at the intersection point of the two beams, then alignment along the optical axes didn't correspond to alignment in the global X-Z plane. This method solves that problem by providing a common register to compare the optical axis of each hologram to.

5. Conclusion

A novel misalignment detection method for orthogonally projected holograms was developed based on the hologram volumes themselves, not on the phase masks that detect them, and the use of a common target to register the hologram centroids to one another. This target was placed at an angle between the two projection directions, and a diffuser was positioned in front of the target to scatter the light from one direction, then the other. A focus scan was then performed to find the Z locations of minimum Shannon entropy for selected X-Y points on the target, indicating that those points were in focus at that Z location. These X-Y-Z points were then paired with their corresponding target frame points, and rigid transformations were calculated with a Procrustes analysis. The final error of these transforms that defined the misalignment was 45.81 µm and 30.43 µm for the left and right transforms, respectively. These values were on the scale of the size of the 10-15 µm diameter point cloud based voxels. The current error ceiling is set by the large area of focus of roughly 1 mm and the large Z sampling interval of 20 µm. Despite these restrictions, both holograms were successfully registered to a common reference frame, and their misalignment values were found. These values will be used in future work to bring the orthogonal holograms into alignment via high resolution stages and print structures.

References

[1] Álvarez-Castaño M I, Madsen A G, Madrid-Wolff J, Sgarminato V, Boniface A, Glückstad J and Moser C 2025 Holographic tomographic volumetric additive manufacturing *Nat. Commun.* **16** 1551

[2] Rietz P, Somers P, Kalt S, Schneider J L G, Kiefer P and Wegener M 2025 Dynamic Multi-Focus 3D Laser Nanoprinting Based on Two-Step Absorption and Computational Holography *Laser Photonics Rev.* **19** 2500187